Science Bulletin 66 (2021) 2115–2123

Contents lists available at ScienceDirect

Science Bulletin

journal homepage: www.elsevier.com/locate/scib

Article

# IL-18 maintains the homeostasis of mucosal immune system via inflammasome-independent but microbiota-dependent manner

Xuesen Zheng [a], Lei Liu [a], Guangxun Meng [b], Shu Zhu [a], Rongbin Zhou [a,c,*], Wei Jiang [a,*]

[a] Hefei National Laboratory for Physical Sciences at Microscale, The CAS Key Laboratory of Innate Immunity and Chronic Disease, School of Basic Medical Sciences, Division of Life Sciences and Medicine, University of Science and Technology of China, Hefei 230027, China

[b] The Center for Microbes, Development and Health, Key Laboratory of Molecular Virology and Immunology, Institut Pasteur of Shanghai, Chinese Academy of Sciences, Shanghai 200031, China

[c] CAS Center for Excellence in Cell and Molecular Biology, University of Science and Technology of China, Hefei 230027, China

ARTICLE INFO

*Article history:*
Received 28 August 2020
Received in revised form 10 November 2020
Accepted 15 January 2021
Available online 26 January 2021

*Keywords:*
Dysbiosis
Immune system
IL-18
Inflammasome

ABSTRACT

Inflammasomes and their product interleukin 18 (IL-18) play important roles in gut microbiota monitoring and homeostasis, and their loss of function could lead to microbiota dysbiosis and accelerate disease progression. However, the impacts of the resulting microbiota dysbiosis on the mucosal immune system are largely unknown. Here, we show that dysbiotic microbiota from *Il18*$^{-/-}$ mice induced immune cell loss in the small intestine (SI) in an inflammasome-independent manner. Cohousing experiments revealed that the immunotoxic phenotype of these microbiota was transferable to wild type (WT) mice and induced immune cell death through the receptor-interacting protein kinase 3 (RIP3)-mixed lineage kinase domain like pseudokinase (MLKL) pathway. Analysis of microbiota composition identified two types of bacteria at the genus level, *Ureaplasma* and *Parasutterella*, that accumulated in *Il18*$^{-/-}$ mice and negatively mediated changes in immune cells in the SI. Furthermore, dysbiosis in *Il18*$^{-/-}$ mice also contributed to increased susceptibility to *Listeria* infection. Collectively, our results demonstrate that IL-18 is essential to microbiota homeostasis and that dysbiotic microbiota could significantly shape the landscape of the immune system.



## 1. Introduction

The gut microbiota plays an important role in the development, differentiation, and homeostasis of intestinal immune cells [1–4]. On the one hand, the gut microbiota is essential for the establishment of a homeostatic gut immune system. Germ-free (GF) mice have fewer and smaller Peyer's patches and fewer immunoglobulin A (IgA)-producing cells than specific pathogen-free (SPF) mice [3,5]. A recent study showed that the viral component of the gut microbiota was essential to the homeostasis of intraepithelial lymphocytes (IELs) [6]. On the other hand, dysbiosis during intestinal inflammation or disease promotes inflammation and worsens the disease. Microbiota from inflammatory bowel disease (IBD) patients promote T helper 17 (Th17) cells differentiation and exacerbate inflammation in the gut [7]. These results indicate that the gut microbiota can maintain immune homeostasis and immune defenses in the gut.

Inflammasomes are cytosolic multiprotein complexes that are formed in response to the recognition of a variety of danger signals from both self (danger-associated molecular patterns, DAMPs) and nonself (pathogen-associated molecular patterns, PAMPs) [8,9]. Upon assembly, the inflammasome triggers the activation of caspase-1, which cleaves proinflammatory IL-1β and IL-18 into active forms and induces pyroptotic cell death. Inflammasomes and their product IL-18 play important roles in monitoring the gut microbiota, and loss of function could lead to an imbalance in the gut microbiota [10,11]. *Nlrp3*$^{-/-}$, *Nlrp6*$^{-/-}$, or *Il18*$^{-/-}$ mice all have been reported to develop dysbiosis in the gut [12–14], although whether NLR family pyrin domain containing 6 (NLRP6) directly regulates the microbiota needs further examination [15,16]. Moreover, dysbiosis resulting from inflammasomes or IL-18 deficiency could dramatically influence the progression of inflammatory diseases. *Il18*$^{-/-}$ mice develop more severe colitis than wild type (WT) mice due to a shift in the microbiota [13]. Furthermore, dysbiosis resulting from NLRP6 deficiency leads to increased susceptibility to colorectal tumorigenesis [17]. These results indicate that dysbiosis caused by inflammasomes or IL-18 can modulate the immune defense and homeostasis of the

* Corresponding authors.
*E-mail addresses:* zrb1980@ustc.edu.cn (R. Zhou), ustcjw@ustc.edu.cn (W. Jiang).

https://doi.org/10.1016/j.scib.2021.01.025
2095-9273/

gut; however, the mechanisms involved in this process remain unknown.

Here, we investigated changes in the intestinal immune system in inflammasomes and IL-18-deficient mice and the mechanisms underlying these alterations. We discovered that in the small intestine (SI), dysbiotic microbiota in *Il18*$^{-/-}$ mice caused immune cell death via the necrotic pathway in an inflammasome-independent manner. Our data also demonstrated that *Il18*$^{-/-}$ mice were more susceptible to *Listeria* infection, highlighting the importance of host microbiota homeostasis in barrier functions.

## 2. Materials and methods

### 2.1. Mice

*Nlrp3*$^{-/-}$, *Asc*$^{-/-}$, *Il18*$^{-/-}$, *Rip3*$^{-/-}$, and *Mlkl*$^{-/-}$ mice have been previously reported [18–22]. *Nlrp6*$^{-/-}$ mice were provided by Millennium Pharmaceuticals (Cambridge, USA). *Gsdmd*$^{-/-}$ mice were provided by Richard Flavell (Yale University). *Casp1*$^{-/-}$ mice were generated by co-microinjection of Cas9 mRNA and gRNA into the C57BL/6 zygotes. WT mice were purchased from Model Animal Research Center (Nanjing, China). Age and sex matched WT mice were used as controls. All animal experiments were approved by the Ethics Committee of University of Science and Technology of China.

### 2.2. Cell isolation

IELs and lamina propria (LP) were isolated as described previously with minor changes [23]. Briefly, SI or colon was flushed with phosphate buffered solution (PBS) to remove luminal contents, with Peyer's patches excised for SI, opened longitudinally and washed three times with PBS. Intestine was then cut into 1.5–2.0 cm pieces and shaken for 40 min at 37 °C in Hanks balanced salt solutions (HBSS) with 5% fetal bovine serum (FBS). The cell suspensions were purified by density gradient centrifugation with 40%–70% percoll (GE Healthcare, Boston, USA). The remaining tissues were used for LP isolation. Tissues were first shaken 2 × 20 min in HBSS with 5% FBS and 2 mmol/L ethylene diamine tetraacetic acid (EDTA) and then incubated for 20 min in HBSS with 10% FBS and 0.5 mg/mL collagenase IV (Sigma-Aldrich, St. Louis, USA). The tubes were shaken for 10 s. Cell suspensions were filtered and purified by density gradient centrifugation with 40%–80% Percoll. For isolation of cells from spleen, liver, thymus, mesenteric lymph nodes (MLNs), and Peyer's patches, the experiments were performed as previously described [6].

### 2.3. Flow cytometry

Flow cytometry was performed according to standard procedures. The following fluorophore-labeled monoclonal antibodies were used: anti-major histocompatibility complex II (M5/114.15.2) and anti-CD45 (30-F11) from Biolegend (San Diego, USA); anti-T-cell receptor (TCR)αβ (RM4-5), anti-TCR γδ (eBioGL3), anti-B220 (RA3-6B3), anti-NK1.1 (PK136) and anti-CD11c (N418) from Thermo Scientific (Waltham, USA). Samples were processed using a BD FACSVerse instrument (BD, San Jose, USA). Data were analyzed with FlowJo™ Software (version 10.0.7, Tree Star, Franklin Lakes, USA).

### 2.4. Antibiotics treatment

Mice were treated with the following antibiotic cocktails (ABX) for four weeks in their drinking water: ampicillin (Sigma-Aldrich) 1 g/L, vancomycin (Sigma-Aldrich) 0.5 g/L, neomycin (Sigma-Aldrich) 1 g/L, and metronidazole (Sigma-Aldrich) 1 g/L.

### 2.5. Immunofluorescence

The SI (jejunum) or colon tissues were fixed in 4% paraformaldehyde (PFA) for 24 h at 4 °C. After washing three times in PBS, fixed tissues were incubated overnight in PBS with 30% sucrose at 4 °C and then embedded in optimal cutting temperature (OCT) compound [24]. Frozen sections (7 μm) of tissues were blocked with 10% rabbit serum (lysozyme) or 10% rat serum (CD45). For lysozyme, sections were incubated overnight at 4 °C with anti-lysozyme (Abcam, Cambridge, UK) antibody, followed by incubation with fluorescein isothiocyanate (FITC) conjugated secondary antibody (Invitrogen, Carlsbad, USA). CD45 were detected using phycoerythrin (PE) conjugated anti-CD45 (30-F11, Thermo Scientific). Images were counterstained with 4',6-diamidino-2'-phenylindole (DAPI, Invitrogen). Images were acquired with DP72 fluorescence microscopy (Olympus, Tokyo, Japan). The number of CD45$^{+}$ cells per villus were counted.

### 2.6. Hematoxylin-eosin (H&E) and alcian blue/periodic acid-schiffand (AB/PAS) staining

The SI (jejunum) or colon tissues were fixed in 4% paraformaldehyde (PFA) and embedded in paraffin according to standard histological procedures. Sections of 5 μm thickness were stained with H&E or AB/PAS and evaluated under light microscopy.

### 2.7. Western blotting

Freshly harvested SI (jejunum) tissues were placed in NP-40 supplemented with protease inhibitor cocktail (Roche, Basel, Switzerland) at 4 °C. Tissues were then homogenized using Bead-Beater Homogenizers. Suspension was centrifugated at 2000 × *g* for 10 min and supernatant collected and stored at −20 °C until further usage. Protein concentration was determined using a bicinchoninic acid (BCA) protein assay kit (Pierce, Appleton, USA). Same amount of protein was used for each sample. Samples were separated on 15% sodium dodecyl sulfate (SDS)-polyacrylamid gels and the protein was transferred to poly vinylidene fluoride (PVDF) membranes. After blocking, membranes were stained using anti-IL-18 (Biovision, Milpitas, USA), anti-β-actin (Proteintech, Rosemont, USA), or anti-P20 (AdipoGen, San Diego, USA) antibodies and the corresponding second antibodies. Membranes were washed and visualized using ChemiDoc XRS+ system (Bio-Rad, Hercules, USA).

### 2.8. Microbial 16S rRNA sequencing and analysis

Fecal pallets and SI (ileum) contents were collected and stored at −80 °C. The methods used for 16S rRNA sequencing analyses were adapted from the Earth Microbiome Project (EMP, https://earthmicrobiome.org). In brief, bacterial DNA was isolated using QIAamp PowerFecal DNA Kit (Qiagen, Hilden, Germany) and sequenced using Illumina MiSeq (2 × 250 bp) platform (Illumina, San Diego, USA).

Obtained reads were filtered, dereplicated and removed chimeras using the standard DADA2 analysis pipeline [25]. The constructed sequence table was mapped to the optimized SILVA database (version 132, maintained by the DADA2 team). The PHYLOSEQ package in R environment was then used to analyze and visualize the amplicon sequence variant (ASV) table. Linear discriminant analysis of effect size (LEfSe) [26] method was used to find the clades most likely to explain the difference. The threshold on the logarithmic LDA score was set to 3.

### 2.9. Real-time polymerase chain reaction (PCR)

Real-time PCR was performed using SYBR Green Master Mix (Transgen, Beijing, China) on a LightCycler 96 (Roche) to quantify the abundance of *Ureaplasma* and *Parasutterella*. The following primers were used [27]:

*Parasutterella* – forward: 5′ – AACGCGAAAAACCTTACCTACC – 3′;
*Parasutterella* – reverse: 5′ – TGCCCTTTCGTAGCAACTAGTG – 3′;
*Ureaplasma* – forward: 5′ – ATGTGTAGCGGTAAAATGCGTAA – 3′;
*Ureaplasma* – reverse: 5′ – CMTACTTGCGTACGTACTACT – 3′;
16S universal – forward: 5′ – AAACTCAAAKGAATTGACGG – 3′;
16S universal – reverse: 5′ – CTCACRRCACGAGCTGAC – 3′.

### 2.10. Cell survival analysis

Cells were first stained with fluorophore-labeled monoclonal antibodies. After washing, Annexin-V/7-AAD Kit (MultiScience, Hangzhou, China) was then used to detect the survival of cells according to manufacturer's instruction.

### 2.11. Listeria monocytogenes infection

Mice were orally gavaged with approximately $5 \times 10^9$ colony-forming units (CFU) of *Listeria monocytogenes* (*L. monocytogenes*) on day 0. For the quantification of bacterial load, feces, livers, MLNs, and spleens were homogenized in PBS, plated on MacConkey agar (Thermo Scientific) for 2 d at 37 °C, and colonies with white halos were counted at indicated dilution ratio.

### 2.12. Fecal supernatant collection and cell stimulation

Fecal supernatant was prepared as previously described with minor changes [28]. In brief, mice feces were collected freshly and homogenized in PBS (0.4 g/mL). Suspensions underwent 3 serial centrifugations at 3000, 10,000, and 15,000 r/min for 15 min at 4 °C. Supernatant was passed through 0.22 μm filters and stored at −80 °C.

For cell stimulation, spleen cells were isolated as previously described and seeded on a 24 well plate with Opti-MEM (Gibco, Waltham, USA) containing 1% FBS and penicillin/streptomycin. PBS or fecal supernatant was added to the well with a ratio of 1:30. After incubating at 37 °C for 4 h, cells were collected and stained for survival analysis.

For heat treatment experiment, fecal supernatant was boiled at 95 °C for 10 min. After that, cell stimulation was performed as described above.

### 2.13. Statistical analysis

GraphPad Prism (version 8.0.0, GraphPad, San Diego, USA) was used for statistical analysis. Data are expressed as mean ± standard error of the mean (SEM). Student's *t*-test or Mann-Whitney *U*-test was used for two groups comparison. One-way analysis of variance (ANOVA) or Kruskal-Wallis test was used for multiple comparison analysis. $P < 0.05$ were considered significant.

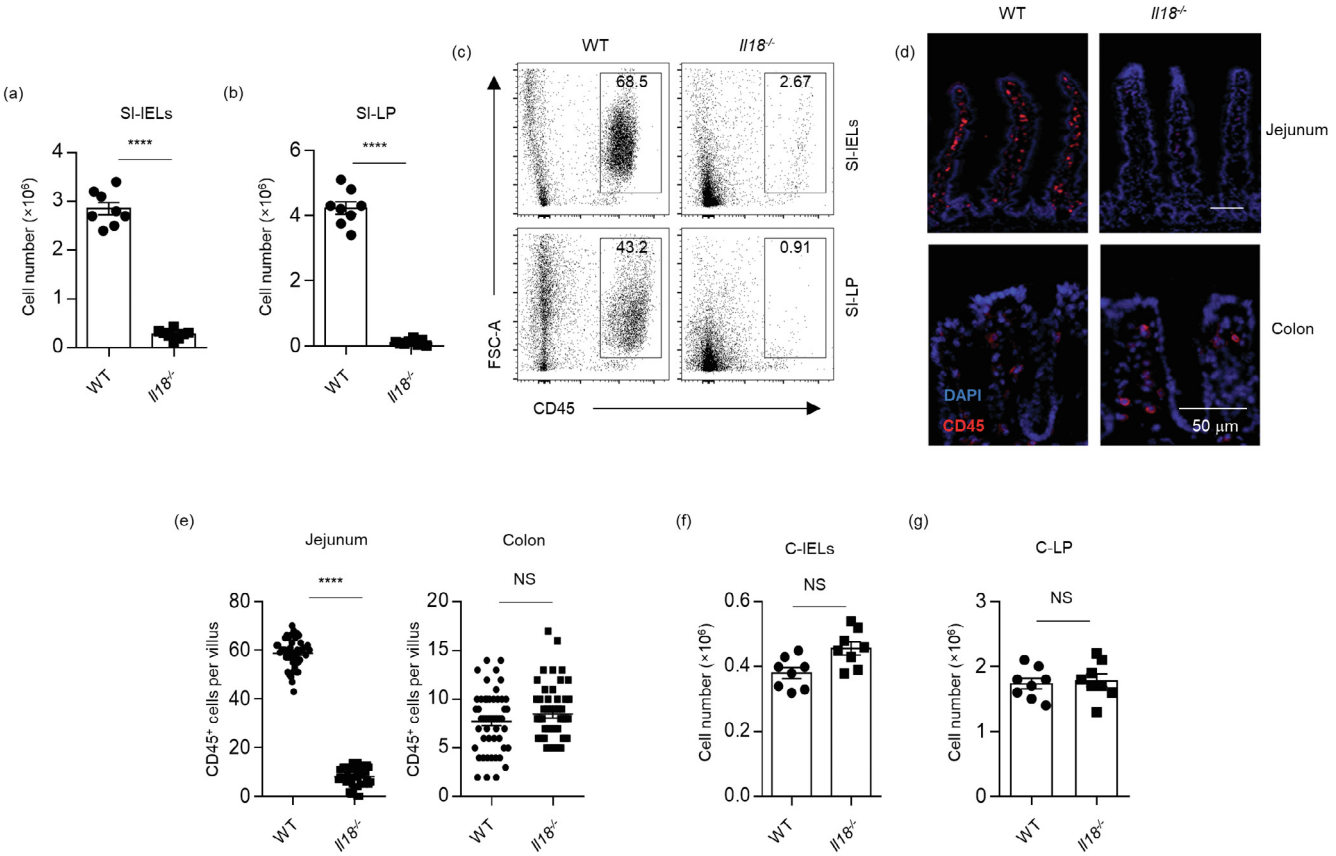


**Fig. 1.** Immune cells were dramatically reduced in the small intestine (SI) of *Il18*$^{-/-}$ mice. (a, b) Total number of CD45$^+$ SI-IELs and SI-LP in WT and *Il18*$^{-/-}$ mice. (c) Representative flow cytometry plots of CD45$^+$ SI-IELs and SI-LP in WT and *Il18*$^{-/-}$ mice. (d) Representative immunofluorescence staining of jejunum and colon sections from indicated mice. DAPI, blue; CD45, red. Scale bar represents 50 μm. (e) Quantification of CD45$^+$ immunofluorescence as in (d), $n = 50$. (f, g) Total number of CD45$^+$ C-IELs and C-LP in WT and *Il18*$^{-/-}$ mice. Data from 2 to 3 independent experiments are shown. Each dot represents one mouse (a, b, f, and g) or villus (e). Data represent mean ± SEM. **** $P < 0.0001$ and NS, not significant.

## 3. Results

### 3.1. Immune cell loss in the SI of *Il18*$^{-/-}$ mice

To explore the role of inflammasomes and IL-18 in intestinal immune homeostasis, we first assessed the number of immune cells in the intestine of *Il18*$^{-/-}$ mice. In the SI, the numbers of CD45$^+$ SI-IELs and SI-LP cells were significantly decreased in *Il18*$^{-/-}$ mice compared with WT mice (Fig. 1a, b). The proportion of CD45$^+$ cells was also dramatically reduced in *Il18*$^{-/-}$ mice (Fig. 1c). Analysis of sections of the SI further confirmed the reduced numbers of CD45$^+$ cells in *Il18*$^{-/-}$ mice (Fig. 1d, e). Such alterations were not observed in the colon of *Il18*$^{-/-}$ mice (Fig. 1f, g). Moreover, the number of major immune cell subsets in the colon of *Il18*$^{-/-}$ mice (C-IELs or C-LP cells) was similar to that in the colon of WT mice (Fig. S1a, b online). We also examined the changes in the number of immune cells in the SI of *Il18*$^{-/-}$ mice at an early age. The numbers of CD45+ SI-IELs and SI-LP cells were comparable between WT and *Il18*$^{-/-}$ mice at the age of 2 weeks (Fig. S1c, d online). Few *Il18*$^{-/-}$ mice showed decreased numbers of CD45$^+$ SI-IELs and SI-LP cells at the age of 3 weeks, while all *Il18*$^{-/-}$ mice exhibited significantly decreased numbers of CD45$^+$ SI-IELs and SI-LP cells at the age of 4 weeks (Fig. S1c, d online). Thus, the loss of immune cells in *Il18*$^{-/-}$ mice started at approximately 3 weeks of age.

Because changes in intestinal immune homeostasis could affect the systematic immune response [3], we next assessed the numbers of immune cells in gut-associated lymphoid tissues (GALTs), including MLNs and Peyer's patches (PPs), and in peripheral tissues, including the spleen, thymus, and liver, of WT and *Il18*$^{-/-}$ mice. The total number of CD45$^+$ cells, as well as major immune cell subsets, in *Il18*$^{-/-}$ mice was similar to that in WT mice among all tissues examined (Fig. S2 online). Thus, the loss of immune cells in *Il18*$^{-/-}$ mice was confined to the SI. These results indicate that IL-18 is important for immune cell homeostasis in the SI.

### 3.2. Immune cell loss in the SI of *Il18*$^{-/-}$ mice is independent of inflammasomes

Bioactive IL-18 is generally considered to be generated via the cleavage of precursor IL-18 upon inflammasome activation [29]. We therefore assessed the changes in the number of immune cells in inflammasome component-deficient mice. Surprisingly, in the SI, the numbers of CD45$^+$ SI-IELs and SI-LP cells from *Nlrp3*$^{-/-}$, *Nlrp6*$^{-/-}$, *Asc*$^{-/-}$, or *Casp1*$^{-/-}$ mice were comparable to those from WT mice (Fig. 2a–c). This discrepancy in small intestinal immune cell numbers between *Il18*$^{-/-}$ mice and mice deficient in the remaining inflammasome components (*Nlrp3*$^{-/-}$, *Nlrp6*$^{-/-}$, *Casp1*$^{-/-}$, and *Asc*$^{-/-}$) led us to assess the amount of IL-18 expressed in intestinal tissues. We measured the expression of active IL-18 in small intestinal tissues from WT, *Casp1*$^{-/-}$, *Asc*$^{-/-}$, and *Il18*$^{-/-}$ mice. Intriguingly, WT, *Casp1*$^{-/-}$, and *Asc*$^{-/-}$ mice had similar expression levels of active IL-18 (Fig. 2d), indicating that IL-18 could be cleaved in an inflammasome-independent manner. Collectively, these results suggest that IL-18 maintains immune cell homeostasis in the SI in an inflammasome-independent manner.

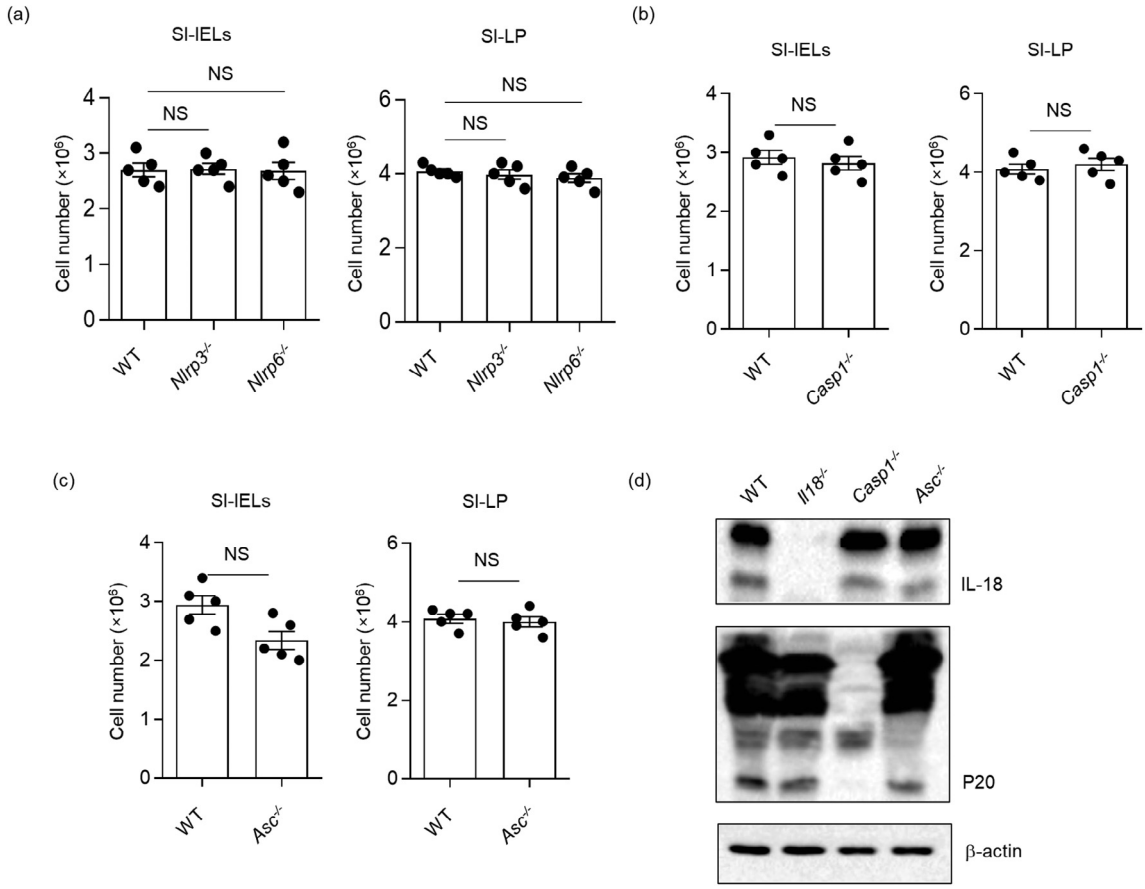


**Fig. 2.** Immune cells loss in the small intestine (SI) of *Il18*$^{-/-}$ mice is independent of inflammasomes. (a–c) Total number of CD45$^+$ SI-IELs and SI-LP in indicated mice. (d) IL-18 expression in jejunum of indicated mice by Western blotting. Data from 2 to 3 independent experiments are shown. Each dot represents one mouse (a–c). Data represent mean ± SEM. NS, not significant.

### 3.3. Immune cell loss in the SI of *Il18*$^{-/-}$ mice is dependent on the microbiota

We next examined the possible cause of the loss of immune cells in the SI in *Il18*$^{-/-}$ mice. *Il18*$^{-/-}$ mice have been reported to have an imbalanced gut microbiota [12]. Considering that the gut microbiota exerts a variety of structural and protective effects on the gut [30], we first assessed whether there were any structural defects in the *Il18*$^{-/-}$ mouse intestine that may lead to an excessive immune response, resulting in intestinal inflammation and immune cell death [31]. H&E staining showed no autoinflammation in the intestines of *Il18*$^{-/-}$ mice (Fig. S3a online). Goblet cells and Paneth cells secrete mucins and antimicrobial peptides, respectively, both of which are essential components of the intestinal barrier [32]. The numbers of goblet cells and Paneth cells in the SI of *Il18*$^{-/-}$ mice were similar to those in WT mice, although goblet cells were dramatically increased in the colon (Fig. S3b, c online). These results suggest that the small intestinal barrier function of *Il18*$^{-/-}$ mice was comparable to that of WT mice.

We next examined whether the loss of immune cells in the SI of *Il18*$^{-/-}$ mice was due to a dysbiotic microbiota by cohousing *Il18*$^{-/-}$ mice with WT mice for 4 weeks. Consistent with our hypothesis, the numbers of CD45$^{+}$ SI-IELs and SI-LP cells were dramatically reduced in cohoused WT (WT(*Il18*$^{-/-}$)) mice (Fig. 3a, b). Analysis of SI sections confirmed the loss of CD45$^{+}$ cells in WT (*Il18*$^{-/-}$) and *Il18*$^{-/-}$(WT) mice (Fig. 3c, d). To further investigate the role of the gut microbiota, we cross-fostered newborn WT mice with *Il18*$^{-/-}$ mothers (CF-WT) and vice versa (CF-*Il18*$^{-/-}$). CF-WT mice had significantly reduced CD45$^{+}$ cells in the SI; however, the number of CD45$^{+}$ cells in the SI of CF-*Il18*$^{-/-}$ mice was comparable to that of WT mice (Fig. 3e–h). Moreover, the immune cells in *Il18*$^{-/-}$ mice could be recovered by feeding the mice ABX water for 4 weeks (Fig. 3i, j). Thus, the microbiota is responsible for the loss of immune cells in *Il18*$^{-/-}$ mice.

### 3.4. Identification of microbiota components that are associated with the loss of immune cell phenotypes

To identify the specific microbiota that are responsible for the loss of immune cells, we performed 16S rRNA amplicon sequencing analysis of feces and small intestinal contents from single-housed and cohoused WT and *Il18*$^{-/-}$ mice. Microbiome communities from WT and *Il18*$^{-/-}$ mice featured distinct clusters in the principal coordinates analysis (PCoA) plot (Fig. 4a), suggesting that the microbiota composition of these mice was different. Importantly, the microbiota of cohoused WT mice were normalized to those of *Il18*$^{-/-}$ mice. We also assessed the diversity of feces and small intestinal microbiomes. The alpha diversity of *Il18*$^{-/-}$ mouse feces was significantly higher than that of WT mouse feces. No significant differences were detected in the SI (Fig. 4b). The microbiome differences between WT and *Il18*$^{-/-}$ mice were also evident at the phylum level. Specifically, the relative abundance of *Verrucomicrobia* in *Il18*$^{-/-}$ mice was dramatically decreased, while *Proteobacteria* and *Tenericutes* were notably increased (Fig. 4c, Table S1 online). Moreover, we found several bacterial taxa at the genus level, such as *Akkermansia* and *Macellibacteroides*, that were

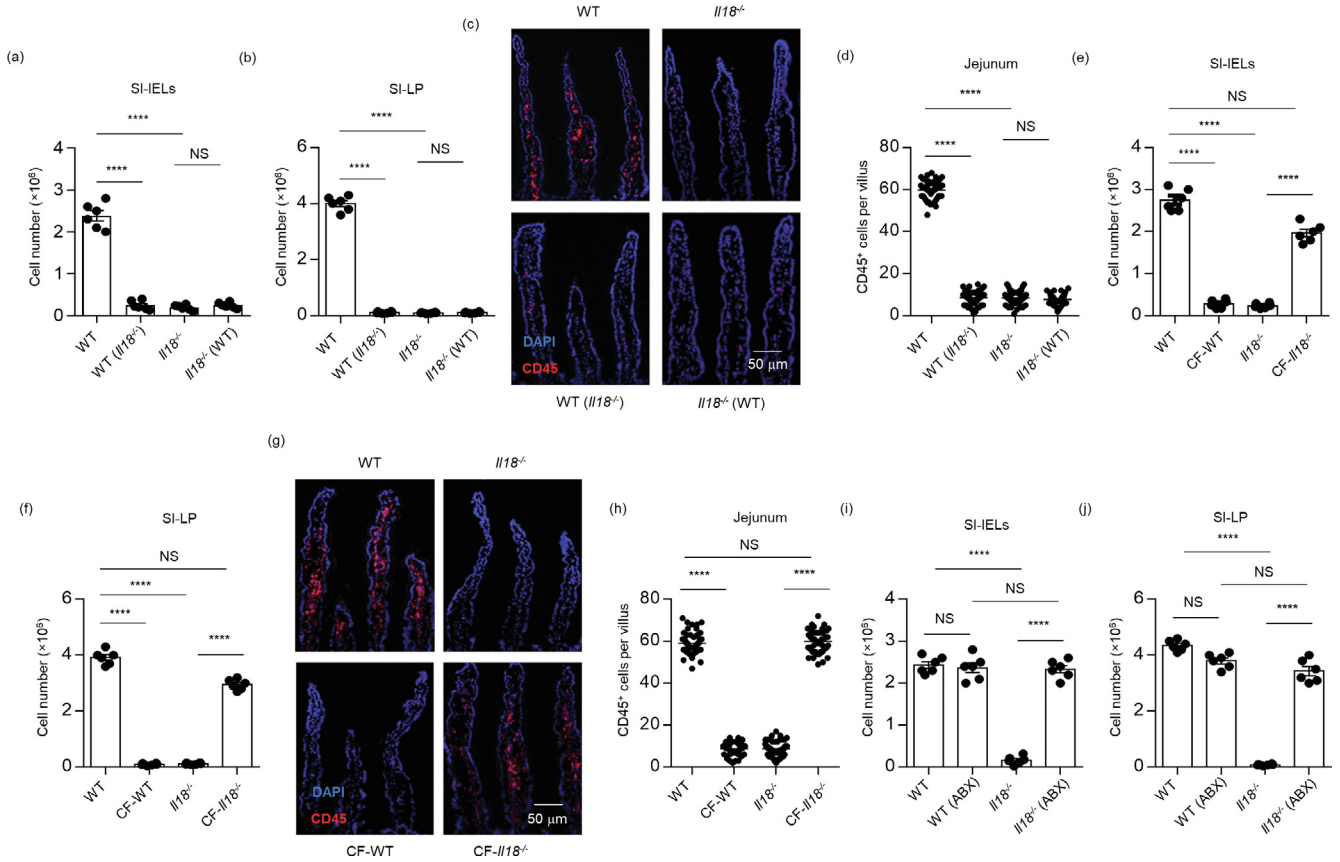


**Fig. 3.** Immune cells loss in the small intestine (SI) of *Il18*$^{-/-}$ mice is transmissible to cohoused or cross-fostered WT mice. (a, b) Total number of CD45$^{+}$ SI-IELs and SI-LP in WT, WT cohoused with *Il18*$^{-/-}$(WT(*Il18*$^{-/-}$)), *Il18*$^{-/-}$ cohoused with WT(*Il18*$^{-/-}$(WT)) and *Il18*$^{-/-}$ mice. (c) Representative immunofluorescence staining of jejunum sections from indicated mice. DAPI, blue; CD45, red. Scale bar represents 50 μm. (d) Quantification of CD45$^{+}$ immunofluorescence as in (c). $n$ = 50. (e, f) Total number of CD45$^{+}$ SI-IELs and SI-LP in WT, WT cross-fostered with *Il18*$^{-/-}$ mother (CF-WT), *Il18*$^{-/-}$ cross-fostered with WT mother (CF-*Il18*$^{-/-}$) and *Il18*$^{-/-}$ mice. (g) Representative immunofluorescence staining of jejunum sections from indicated mice. DAPI, blue; CD45, red. Scale bar represents 50 μm. (h) Quantification of CD45$^{+}$ immunofluorescence as in (g), $n$ = 50. (i, j) Total number of CD45$^{+}$ SI-IELs and SI-LP in indicated mice. Data from 2 to 3 independent experiments are shown. Each dot represents one mouse (a, b, e, f, i, and j) or villus (d, h). Data represent mean ± SEM. **** $P$ < 0.0001 and NS, not significant.

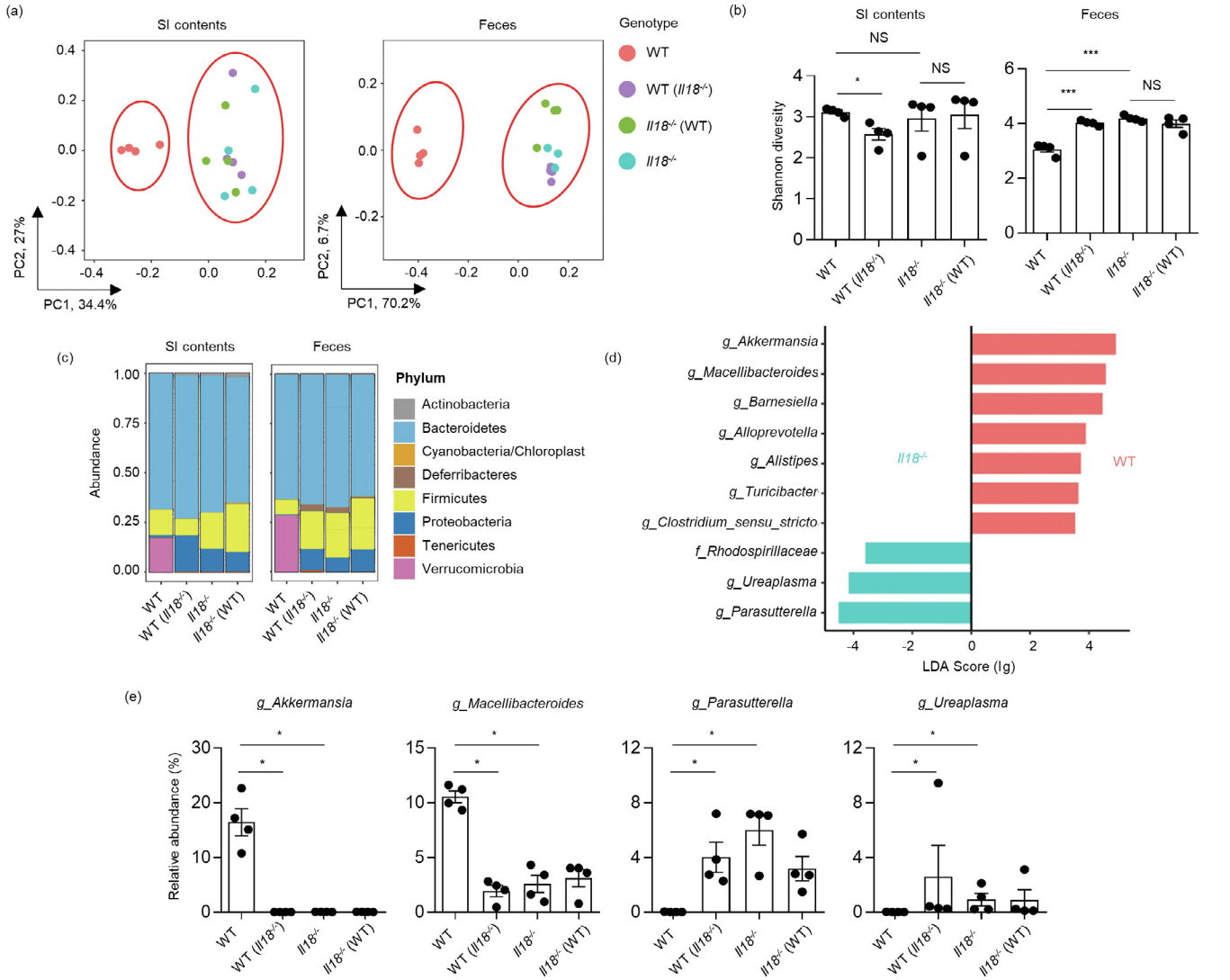


**Fig. 4.** Microbiota profiling in WT and *Il18*$^{-/-}$ mice. (a) Diversity (Shannon index) of gut microbiota from indicated mice. (b) Unweighted UniFrac PCoA of ileum and fecal microbiota harvested from separately housed or cohoused mice. (c) Relative abundance of bacterial phylum from indicated mice. (d) Linear discriminant analysis (LDA) scores of differentially abundant taxa in the ileum microbiomes from WT (green) and *Il18*$^{-/-}$ (red) mice. Length indicates effect size associated with a taxon. $P = 0.05$ for the Kruskal-Wallis H statistic; LDA score >3. (e) Relative abundance of top differentially abundant taxa identified by LDA from indicated mice. Each dot represents one mouse (a, b, and e). Data represent mean ± SEM. * $P < 0.05$, *** $P < 0.001$, **** $P < 0.0001$, and NS, not significant.

significantly enriched in WT mice, as well as a few other taxa, including *Ureaplasma* and *Parasutterella*, that were significantly enriched in *Il18*$^{-/-}$ mice (Fig. 4d, e, and Fig. S4 online) using LEfSe.

We next sought to determine the bacteria that cosegregated with the loss of immune cells in the SI by combining the LEfSe results and their relative abundances in cohoused mice. Considering that CD45$^{+}$ cells were recovered in *Il18*$^{-/-}$ mice after treatment with ABX (Fig. 3i, j), we focused on the ASVs that were overrepresented in *Il18*$^{-/-}$ mice. The results showed that *Ureaplasma* and *Parasutterella* were significantly increased in WT (*Il18*$^{-/-}$) mice, while *Rhodospirillaceae* only showed an increase in *Il18*$^{-/-}$ mice (Fig. 4d, e, and Fig. S4a–g online). Collectively, these results suggest that the bacterial taxa *Ureaplasma* and *Parasutterella* might be the main causes of immune cell loss in *Il18*$^{-/-}$ mice.

### *3.5. Microbiota from Il18*$^{-/-}$ *mice induce immune cell death through the receptor-interacting protein kinase 3 (RIP3)-mixed lineage kinase domain like pseudokinase (MLKL) pathway*

Given the marked reduction in CD45$^{+}$ cells in the SI of *Il18*$^{-/-}$ mice, we performed cell survival analysis of these cells from WT and *Il18*$^{-/-}$ mice. Surprisingly, almost all the immune cells isolated from the SI of *Il18*$^{-/-}$ mice were necrotic (Fig. 5a, b). Considering the predominant phenotype of the microbiota of *Il18*$^{-/-}$ mice (Fig. 4a), we sought to determine the mechanisms of immune cell death by cohousing *Il18*$^{-/-}$ mice with mice deficient in several types of cell death. Pyroptosis and necroptosis are the two most common forms of necrotic cell death [33]. We first assessed the possible role of pyroptosis in immune cell death using *Gsdmd*$^{-/-}$ mice [34]. While the numbers of CD45$^{+}$ SI-IELs and SI-LP cells in *Gsdmd*$^{-/-}$ mice were also comparable to those in WT mice, the numbers were significantly reduced after the mice were cohoused with *Il18*$^{-/-}$ mice (Fig. S5 online). Thus, the loss of immune cells in *Il18*$^{-/-}$ mice does not occur through pyroptotic cell death. Receptor-interacting serine-threonine kinase 3 (RIP3) and mixed lineage kinase domain-like protein (MLKL) are two critical regulatory proteins associated with necroptosis [35]. The numbers of CD45$^{+}$ SI-IELs and SI-LP cells in *Rip3*$^{-/-}$ or *Mlkl*$^{-/-}$ mice were similar to those in WT mice and were unaltered even after the mice were cohoused with *Il18*$^{-/-}$ mice (Fig. 5c, d). Moreover, the real-time PCR results showed significant increases in the relative 16S rRNA copies of *Ureaplasma* or *Parasutterella* in both cohoused

*Rip3*$^{-/-}$ and cohoused *Mlkl*$^{-/-}$ mice (Fig. S6 online). Therefore, the dysbiotic microbiota in *Il18*$^{-/-}$ mice induces immune cell death through the RIP3-MLKL pathway.

To further confirm this hypothesis, we assessed the ability of WT and *Il18*$^{-/-}$ mouse fecal supernatant (FS) to induce immune cell death *in vitro*. Briefly, isolated splenic immune cells were cultured with FS from WT or *Il18*$^{-/-}$ mice for 4 h, and the viability of the cells was analyzed by flow cytometry. Consistent with the above findings, the frequency of necrotic cells was significantly increased in WT mice after culture with *Il18*$^{-/-}$ mouse FS compared to WT mouse FS, and it was comparable in *Mlkl*$^{-/-}$ and *Rip3*$^{-/-}$ mice (Fig. 5e, f). Moreover, adding Q-VD-OPh, a pancaspase inhibitor, to the FS of *Il18*$^{-/-}$ mice did not decrease the frequency of necrotic cells (Fig. S7 online), indicating that the immune cells in the SI of *Il18*$^{-/-}$ mice indeed undergo necrotic cell death. Collectively, these findings indicate that the dysbiotic microbiota of *Il18*$^{-/-}$ mice induce necrotic immune cell death through the RIP3-MLKL pathway.

### *3.6. Microbiota dysbiosis contributes to the increased susceptibility of Il18*$^{-/-}$ *mice to Listeria infection*

Because the gut microbiota plays an important role in helping the body control pathogen expansion [36,37], we next investigated whether dysbiosis in *Il18*$^{-/-}$ mice could affect host defense against orally administered *L. monocytogenes*. *Il18*$^{-/-}$ mice exhibited reduced clearance of *Listeria*, as evidenced by markedly increased body weight loss (Fig. 6a) and *Listeria* CFU in the spleen, liver and MLNs (Fig. 6b–d) after 72 h of infection compared to those of WT mice. Moreover, these trends resembled those in WT (*Il18*$^{-/-}$) mice (Fig. 6a–d). Collectively, these results suggested that a dysbiotic microbiota increases the susceptibility of *Il18*$^{-/-}$ mice to *Listeria* infection.

## 4. Discussion and conclusion

In the present study, we investigated the impacts of dysbiosis on the homeostasis of the immune system in the gut. Mice deficient in IL-18 developed a dysbiotic microbiota in the gut, causing immune cell death in the SI via the RIP3-MLKL pathway. Moreover, dysbiosis and disruption of the immune system increased the vulnerability of the host to infection. Thus, our data provided evidence that dysbiosis could strongly influence the homeostasis of the immune system.

Our data showed that *Il18*$^{-/-}$ mice lost immune cells in the SI in a microbiota-dependent manner but had a normal number of immune cells in the colon. Furthermore, the main microbial composition of the colon was similar to that of the intestine. One possible explanation for this discrepancy in immune system changes may be the anatomical differences between the SI and colon. The SI only has one easily removable layer of mucus; in contrast, the colon has a two-layer mucus system, with dense inner mucus and loose outer mucus [38,39]. The dense inner mucus in the colon

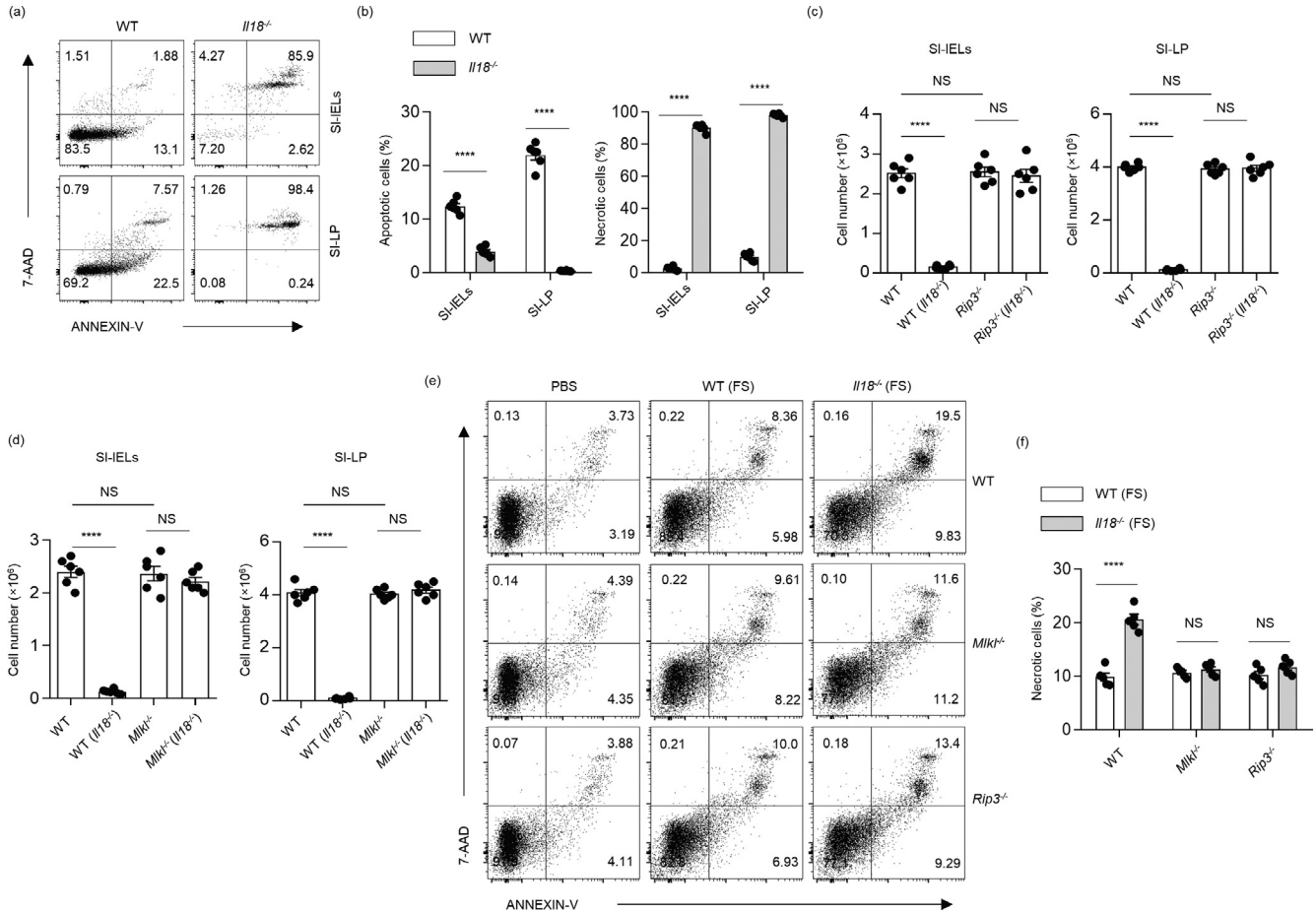


**Fig. 5.** Immune cells loss in the small intestine (SI) of *Il18*$^{-/-}$ mice depends on the RIP3-MLKL pathway. (a) Representative flow cytometry plots and (b) frequency of apoptotic (ANNEXIN V$^{+}$7-AAD$^{-}$) and necrotic (ANNEXIN V$^{+}$7-AAD$^{+}$) CD45$^{+}$ cells from SI of WT and *Il18*$^{-/-}$ mice. (c, d) Total number of CD45$^{+}$ SI-IELs and SI-LP in indicated mice. (e) Representative flow cytometry plots and (f) frequency of necrotic spleen CD45$^{+}$ cells from indicated mice after culturing in WT or *Il18*$^{-/-}$ mice fecal supernatant for 4 h. Data from 2 to 3 independent experiments are shown. Each dot represents one mouse (b–d). Data represent mean ± SEM. **** $P < 0.0001$ and NS, not significant.

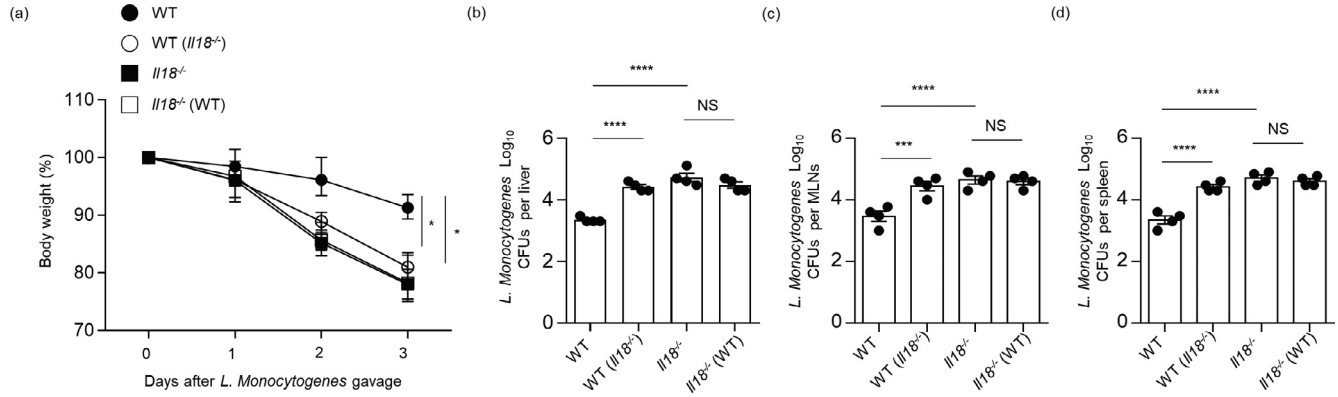


**Fig. 6.** Microbiota dysbiosis contributes to the increased susceptibility of *Il18*$^{-/-}$ mice to *Listeria* infection. (a) Percentage of weight change after infection from indicated mice. (b–d) *Listeria* CFU in liver (b), MLNs (c), and spleen (d) from indicated mice 72 h after infection. Data from 2 to 3 independent experiments are shown. Each dot represents one mouse. Data represent mean ± SEM. * $P < 0.05$, *** $P < 0.001$, **** $P < 0.0001$, and NS, not significant.

could prevent the pathogenic microbiota from accessing immune cells in the epithelium and lamina propria.

IL-18 is generally considered to be processed by caspase 1 and becomes active; however, we detected active IL-18 in the intestine, even in *Casp1*$^{-/-}$ and *Asc*$^{-/-}$ mice. Active IL-18 was also detected in the colon of *Casp1/11*$^{-/-}$ mice [40], suggesting an inflammasome-independent form of IL-18 activation. Indeed, Fas stimulation could induce the release of active IL-18 in caspase 1-deficient macrophages but not in caspase 8-deficient macrophages, indicating that caspase 8 could process IL-18 [29]. However, the enzyme responsible for active IL-18 production in the intestine still needs to be explored.

Using 16S rRNA sequencing technology, we identified two types of bacteria at the genus level that were highly likely to be the cause of the loss of immune cells in the *Il18*$^{-/-}$ mouse SI: *Ureaplasma* and *Parasutterella*. Indeed, both *Ureaplasma* and *Parasutterella* have been recognized as opportunistic pathogens [41–43], that could potentially disturb immune cell homeostasis. Notably, CF-*Il18*$^{-/-}$ mice have a similar number of CD45$^{+}$ cells in the SI as WT mice. Real-time PCR analysis revealed that the relative 16S rRNA copies of *Ureaplasma* and *Parasutterella* in CF-*Il18*$^{-/-}$ mice were similar to those in normally reared WT mice (Fig. S8 online). We hypothesized that IL-18 deficiency in mice leads to increased vulnerability to the colonization and expansion of the opportunistic pathogens *Ureaplasma* and *Parasutterella*. Additionally, isolating and transferring *Ureaplasma* and *Parasutterella* into SPF mice would provide more direct evidence to support this conclusion.

Considering that the microbial compositions of the SI and colon were similar, fecal supernatant (FS) was used to confirm the necrotic death of immune cells in the SI of *Il18*$^{-/-}$ mice. However, the molecules that induce immune cell death are still unclear. The immunotoxic phenotype of FS from *Il18*$^{-/-}$ mice was abolished when subjected to heat treatment (Fig. S9 online). Thus, we hypothesized that the toxin proteins secreted by these bacteria are probable candidates [44]. For example, one species from the genus *Parasutterella*, *Parasutterella excrementihominis*, could produce the virulence factor hemolysin, which is toxic to erythrocytes and leukocytes [45]. This property of the virulence factor could also explain why the epithelial structure of the SI in *Il18*$^{-/-}$ mice was comparable to that in WT mice.

Previous studies have shown that inflammasomes contribute to host protection against infection by inducing the secretion of IL-1β and IL-18 [46–48]. However, the role of dysbiotic microbiota development in these gene knockout mice during infection remains unknown. Our results indicated that the dysbiotic microbiota from *Il18*$^{-/-}$ mice could exacerbate intestinal *Listeria* infection, possibly through disrupting the immune system in the SI.

Collectively, our findings demonstrate that dysbiotic microbiota could have a profound impact on intestinal immune system homeostasis. Understanding how microbiota influence the immune system, whether under homeostasis or imbalance, could provide new insights for the treatment of intestinal diseases, such as infectious diseases, cancer, or IBD.

## Conflict of interest

The authors declare that they have no conflict of interest.

## Acknowledgments

This work was supported by the National Key Research and Development Program of China (2020YFA0509101), the National Natural Science Foundation of China (91742202, 81722022, and 81821001), and the Young Talent Support Program and Fundamental Research Funds for the Central Universities and the University Synergy Innovation Program of Anhui Province (GXXT-2019-026).

## Author contributions

Guangxun Meng, Shu Zhu, Rongbin Zhou, and Wei Jiang designed the experiments. Xuesen Zheng and Lei Liu performed the experiments. Xuesen Zheng, Wei Jiang, and Rongbin Zhou analyzed the data. Xuesen Zheng and Rongbin Zhou wrote the manuscript. Wei Jiang reviewed and edited the manuscript. Rongbin Zhou and Wei Jiang supervised the project.

## Appendix A. Supplementary materials

Supplementary materials to this article can be found online at https://doi.org/10.1016/j.scib.2021.01.025.

## References

[1] Belkaid Y, Hand TW. Role of the microbiota in immunity and inflammation. Cell 2014;157:121–41.
[2] Round JL, Mazmanian SK. The gut microbiota shapes intestinal immune responses during health and disease. Nat Rev Immunol 2009;9:313–23.
[3] Macpherson AJ, Harris NL. Interactions between commensal intestinal bacteria and the immune system. Nat Rev Immunol 2004;4:478–85.
[4] Hooper LV, Littman DR, Macpherson AJ. Interactions between the microbiota and the immune system. Science 2012;336:1268–73.
[5] Macpherson AJ, Hunziker L, McCoy K, et al. IgA responses in the intestinal mucosa against pathogenic and non-pathogenic microorganisms. Microbes Infect 2001;3:1021–35.
[6] Liu L, Gong T, Tao W, et al. Commensal viruses maintain intestinal intraepithelial lymphocytes via noncanonical RIG-I signaling. Nat Immunol 2019;20:1681–91.

[7] Britton GJ, Contijoch EJ, Mogno I, et al. Microbiotas from humans with inflammatory bowel disease alter the balance of gut Th17 and RORγt+ regulatory T cells and exacerbate colitis in mice. Immunity 2019;50:212–24.
[8] Martinon F, Mayor A, Tschopp J. The inflammasomes: guardians of the body. Annu Rev Immunol 2009;27:229–65.
[9] Gong T, Liu L, Jiang W, et al. DAMP-sensing receptors in sterile inflammation and inflammatory diseases. Nat Rev Immunol 2020;20:95–112.
[10] Man SM. Inflammasomes in the gastrointestinal tract: infection, cancer and gut microbiota homeostasis. Nat Rev Gastroenterol Hepatol 2018;15:721–37.
[11] Levy M, Thaiss CA, Katz MN, et al. Inflammasomes and the microbiota–partners in the preservation of mucosal homeostasis. Semin Immunopathol 2015;37:39–46.
[12] Elinav E, Strowig T, Kau AL, et al. NLPR6 inflammasome regulates colonic microbial ecology and risk for colitis. Cell 2011;145:745–57.
[13] Levy M, Thaiss CA, Zeevi D, et al. Microbiota-modulated metabolites shape the intestinal microenvironment by regulating NLRP6 inflammasome signaling. Cell 2015;163:1428–43.
[14] Zaki MH, Boyd KL, Vogel P, et al. The NLPR3 inflammasome protects against loss of epithelial integrity and mortality during experimental colitis. Immunity 2010;32:379–91.
[15] Lemire P, Robertson SJ, Maughan H, et al. The NLR protein NLRP6 does not impact gut microbiota composition. Cell Rep 2017;21:3653–61.
[16] Mamantopoulos M, Ronchi F, Van Hauwermeiren F, et al. Nlrp6- and ASC-dependent inflammasomes do not shape the commensal gut microbiota composition. Immunity 2017;47:339–48.
[17] Normand S, Delanoye-Crespin A, Bressenot A, et al. Nod-like receptor pyrin domain-containing protein 6 (NLRP6) controls epithelial self-renewal and colorectal carcinogenesis upon injury. Proc Natl Acad Sci USA 2011;108:9601–6.
[18] Wu J, Huang Z, Ren J, et al. *Mlkl* knockout mice demonstrate the indispensable role of Mlkl in necroptosis. Cell Res 2013;23:994–1006.
[19] Takeda K, Tsutsui H, Yoshimoto T, et al. Defective NK cell activity and TH1 response in IL-18-deficient mice. Immunity 1998;8:383–90.
[20] Newton K, Sun X, Dixit VM. Kinase RIP3 is dispensable for normal NF-κBs, signaling by the B-cell and T-cell receptors, tumor necrosis factor receptor 1, and Toll-like receptors 2 and 4. Mol Cell Biol 2004;24:1464–9.
[21] Mariathasan S, Newton K, Monack DM, et al. Differential activation of the inflammasome by caspase-1 adaptors ASC and Ipaf. Nature 2004;430:213–8.
[22] Martinon F, Petrilli V, Mayor A, et al. Gout-associated uric acid crystals activate the NALP3 inflammasome. Nature 2006;440:237–41.
[23] Jiang W, Wang X, Zeng B, et al. Recognition of gut microbiota by NOD2 is essential for the homeostasis of intestinal intraepithelial lymphocytes. J Exp Med 2013;210:2465–76.
[24] Wang S, Xia P, Chen Y, et al. Regulatory innate lymphoid cells control innate intestinal inflammation. Cell 2017;171:201–16.
[25] Callahan BJ, McMurdie PJ, Rosen MJ, et al. DADA2: high-resolution sample inference from illumina amplicon data. Nat Methods 2016;13:581–3.
[26] Segata N, Izard J, Waldron L, et al. Metagenomic biomarker discovery and explanation. Genome Biol 2011;12:R60.
[27] Yang Y-W, Chen M-K, Yang B-Y, et al. Use of 16S rRNA gene-targeted group-specific primers for real-time PCR analysis of predominant bacteria in mouse feces. Appl Environ Microbiol 2015;81:6749–56.
[28] Meelu P, Marin R, Clish C, et al. Impaired innate immune function associated with fecal supernatant from Crohn's disease patients: insights into potential pathogenic role of the microbiome. Inflamm Bowel Dis 2014;20:1139–46.
[29] Afonina IS, Muller C, Martin SJ, et al. Proteolytic processing of interleukin-1 family cytokines: variations on a common theme. Immunity 2015;42:991–1004.
[30] O'Hara AM, Shanahan F. The gut flora as a forgotten organ. EMBO Rep 2006;7:688–93.
[31] Cohen JJ, Duke RC, Fadok VA, et al. Apoptosis and programmed cell death in immunity. Annu Rev Immunol 1992;10:267–93.
[32] Peterson LW, Artis D. Intestinal epithelial cells: regulators of barrier function and immune homeostasis. Nat Rev Immunol 2014;14:141–53.
[33] Berghe TV, Linkermann A, Jouan-Lanhouet S, et al. Regulated necrosis: the expanding network of non-apoptotic cell death pathways. Nat Rev Mol Cell Biol 2014;15:135–47.
[34] Shi J, Zhao Y, Wang K, et al. Cleavage of GSDMD by inflammatory caspases determines pyroptotic cell death. Nature 2015;526:660–5.
[35] Sun L, Wang H, Wang Z, et al. Mixed lineage kinase domain-like protein mediates necrosis signaling downstream of RIP3 kinase. Cell 2012;148:213–27.
[36] Rivera-Chavez F, Zhang LF, Faber F, et al. Depletion of butyrate-producing *Clostridia* from the gut microbiota drives an aerobic luminal expansion of *Salmonella*. Cell Host Microbe 2016;19:443–54.
[37] Tanoue T, Morita S, Plichta DR, et al. A defined commensal consortium elicits CD8 T cells and anti-cancer immunity. Nature 2019;565:600–5.
[38] Johansson ME, Sjovall H, Hansson GC. The gastrointestinal mucus system in health and disease. Nat Rev Gastroenterol Hepatol 2013;10:352–61.
[39] Mowat AM, Agace WW. Regional specialization within the intestinal immune system. Nat Rev Immunol 2014;14:667–85.
[40] Volk JK, Nystrom EEL, van der Post S, et al. The Nlrp6 inflammasome is not required for baseline colonic inner mucus layer formation or function. J Exp Med 2019;216:2602–18.
[41] Shin NR, Whon TW, Bae JW. Proteobacteria: microbial signature of dysbiosis in gut microbiota. Trends Biotechnol 2015;33:496–503.
[42] Silwedel C, Haarmann A, Fehrholz M, et al. More than just inflammation: *Ureaplasma* species induce apoptosis in human brain microvascular endothelial cells. J Neuroinflammation 2019;16:38.
[43] Gassiep I, Gore L, Dale JL, et al. *Ureaplasma urealyticum* necrotizing soft tissue infection. J Infect Chemother 2017;23:830–2.
[44] Sridharan H, Upton JW. Programmed necrosis in microbial pathogenesis. Trends Microbiol 2014;22:199–207.
[45] Cavalieri SJ, Snyder IS. Effect of *Escherichia coli* alpha-hemolysin on human peripheral leukocyte viability *in vitro*. Infect Immun 1982;36:455–61.
[46] Miao EA, Leaf IA, Treuting PM, et al. Caspase-1-induced pyroptosis is an innate immune effector mechanism against intracellular bacteria. Nat Immunol 2010;11:1136–42.
[47] Kim S, Bauernfeind F, Ablasser A, et al. *Listeria monocytogenes* is sensed by the NLRP3 and AIM2 inflammasome. Eur J Immunol 2010;40:1545–51.
[48] Wlodarska M, Thaiss CA, Nowarski R, et al. NLRP6 inflammasome orchestrates the colonic host-microbial interface by regulating goblet cell mucus secretion. Cell 2014;156:1045–59.

Xuesen Zheng is a Ph.D. candidate at the School of Basic Medical Sciences, University of Science and Technology of China. His research interest focuses on how pattern recognition receptors (PRRs) regulate the homeostasis of gut microbiota.

Rongbin Zhou is a professor at the School of Basic Medical Sciences, University of Science and Technology of China. He studies the mechanisms of PRRs activation, neuro-immune interactions, immune-metabolic interactions, and strategies to treat inflammation-related diseases.

Wei Jiang is a professor at the School of Basic Medical Sciences, University of Science and Technology of China. She studies the mechanisms of PRRs activation and their role in regulating the homeostasis of the intestinal mucosa.